



The official journal of

INTERNATIONAL FEDERATION OF PIGMENT CELL SOCIETIES · SOCIETY FOR MELANOMA RESEARCH

PIGMENT CELL & MELANOMA Research

Segregation Between an Ornamental and a Disease Driver Gene Provides Insights Into Pigment Cell Regulation

Erika Soria¹ | Qiusheng Lu² | Will Boswell¹ | Kang Du¹ |
Yanting Xing¹  | Mikki Boswell¹ | Korri S. Weldon³ |
Zhao Lai^{3,4} | Markita Savage¹ | Manfred Scharl^{1,5,6} |
Yuan Lu¹ 

DOI: 10.1111/pcmr.13196

Volume 38, Issue 1, Pages 1-13



If you wish to order reprints of this article,
please see the guidelines [here](#)

Supporting Information for this article is freely available [here](#)

EMAIL ALERTS

Receive free email alerts and stay up-to-date on what is published
in Pigment Cell & Melanoma Research – [click here](#)

Submit your next paper to PCMR online at <http://mc.manuscriptcentral.com/pcmr>

Subscribe to PCMR and stay up-to-date with the only journal committed to publishing
basic research in melanoma and pigment cell biology



As a member of the IFPCS or the SMR you automatically get online access to PCMR. Sign up as
a member today at www.ifpcs.org or at www.societymelanomaresarch.org

To take out a personal subscription, please [click here](#)

More information about Pigment Cell & Melanoma Research at www.pigment.org

ORIGINAL ARTICLE OPEN ACCESS

Segregation Between an Ornamental and a Disease Driver Gene Provides Insights Into Pigment Cell Regulation

Erika Soria¹ | Qiusheng Lu² | Will Boswell¹ | Kang Du¹ | Yanting Xing¹  | Mikki Boswell¹ | Korri S. Weldon³ | Zhao Lai^{3,4} | Markita Savage¹ | Manfred Schartl^{1,5,6} | Yuan Lu¹ 

¹The Xiphophorus Genetic Stock Center, Texas State University, San Marcos, Texas, USA | ²Beijing No. 7 Middle School, Beijing, China | ³Greehey Children's Cancer Research Institute, University of Texas Health Science Center, San Antonio, Texas, USA | ⁴Department of Molecular Medicine, University of Texas Health Science Center, San Antonio, Texas, USA | ⁵Developmental Biochemistry, Biocenter, University of Würzburg, Würzburg, Germany | ⁶Research Department for Limnology, University of Innsbruck, Mondsee, Austria

Correspondence: Yuan Lu (y_l54@txstate.edu)

Received: 22 May 2024 | **Revised:** 18 July 2024 | **Accepted:** 19 August 2024

Funding: This work was supported by Cancer Prevention and Research Institute of Texas, National Institutes of Health and Texas State University.

Keywords: evolution | genetics | hybrid incompatibility | hybridization | *Xiphophorus*

ABSTRACT

Genetic interactions are adaptive within a species. Hybridization can disrupt such species-specific genetic interactions and creates novel interactions that alter the hybrid progeny overall fitness. Hybrid incompatibility, which refers to degenerative genetic interactions that decrease the overall hybrid survival and sterility, is one of the results from combining two diverged genomes in hybrids. The discovery of spontaneous lethal tumorigenesis and underlying genetic interactions in select hybrids between diverged *Xiphophorus* species showed that lethal pathological process can result from degenerative genetic interactions. Such genetic interactions leading to lethal phenotype are thought to shield gene flow between diverged species. However, hybrids between certain *Xiphophorus* species do not develop such tumors. Here we report the identification of a locus residing in the genome of one *Xiphophorus* species that represses an oncogene from a different species. Our finding provides insights into normal and pathological pigment cell development, regulation and a molecular mechanism in hybrid incompatibility.

1 | Introduction

The genome incompatibility hypothesis stated by Dobzhansky–Muller (DM) describes how negative genetic interactions in hybrids can serve as the molecular mechanisms accounting for hybrid incompatibility (Bateson 1909; Dobzhansky 1937; Muller 1940; Coyne 2004; Mack and Nachman 2017). Almost a century ago, three independent studies found that interspecies hybrids between southern platyfish *Xiphophorus maculatus* (*X. maculatus*) and green swordtail *X. hellerii* develop spontaneous melanoma (Haiissler 1928; Gordon 1927; Kosswig 1928). This fish model represents one of the examples supporting the DM incompatibility hypothesis (Maheshwari and Barbash 2011; Pennisi 2006; Noor 2003). The *X. maculatus* exhibits a nevus-like

black pigmentation pattern (*Spotted dorsal*, or *Sd*), and a red pigmentation pattern (*Dorsal red*, or *Dr*) in the dorsal fin, while the *X. hellerii* exhibits neither trait. In hybrids between the *X. maculatus* and *X. hellerii*, the *Sd* and *Dr* pigmentation pattern becomes enhanced and expanded. The *Sd* pattern covers the entire dorsal fin and *Dr* pattern expands to the tail fin and posterior of the body side (Schartl and Lu 2024; Lu, Sandoval, et al. 2020). In the backcross hybrid using the *Sd* and *Dr* negative species (i.e., *X. hellerii*) as recurrent parental, 50% of the hybrids inherited recurrent parental species pigmentation pattern (i.e., no *Sd*, nor *Dr*), 25% of hybrids exhibit an F_1 -like *Sd* pattern, and 25% exhibit invasive and lethal nodular exophytic melanoma (Schartl and Lu 2024; Lu, Sandoval, et al. 2020; Schartl and Walter 2016). The *Dr* pattern never progressed to a pathological condition.

This is an open access article under the terms of the [Creative Commons Attribution-NonCommercial](https://creativecommons.org/licenses/by-nc/4.0/) License, which permits use, distribution and reproduction in any medium, provided the original work is properly cited and is not used for commercial purposes.

© 2024 The Author(s). *Pigment Cell & Melanoma Research* published by John Wiley & Sons Ltd.

Summary

- The Dobzhansky–Muller model states that epistatic interactions between genes in diverged species underlies hybrid incompatibility.
- There are a few vertebrate interspecies hybrid cases that support the Dobzhansky–Muller model.
- This study reports a fish hybrid system where incompatible genetic interactions are involved in neuronal regulation of pigment cell biology, and also identifies a novel point of regulation for pigment cells.

It has been found that the *X. maculatus* *Sd*, the enhanced *Sd* pattern in the F₁ hybrid, and melanoma in the backcross hybrids is driven by a mutant duplicate copy of epidermal growth factor receptor (EGFR) that is termed *Xiphophorus Melanoma Receptor Tyrosine Kinase (xmrk)* (Adam, Dimitrijevic, and Schartl 1993; Wittbrodt et al. 1989). The expressivity of *Sd*, however, is regulated by copy number of a co-evolved *xmrk* regulator in *X. maculatus*. With two copies of the *xmrk* regulator, *Sd* is restricted to a nevus-like pigmentation dot, while losing the *xmrk* regulators through hybridization leads to pigment cell benign hyperplasia (losing one copy of the regulator), and melanoma (losing both copies of the regulator). The *xmrk* regulator has recently been mapped to chromosome 5 of *X. maculatus* genome (Lu, Sandoval, et al. 2020).

The *Sd* and *Dr* loci in the *X. maculatus* offer a naturally occurred genetic system by which an oncogene activity can be assessed by phenotyping pigmentation patterns. The *Dr* is thought to be tightly linked to *Sd* as *Dr* co-segregates with *Sd* in the *X. maculatus*–*X. hellerii* hybrids. However, the *Dr* does not exhibit an *Sd*-like dosage effect from the *xmrk* regulator. The *Sd* is a melanophore phenotype, while the *Dr* is composed of xanthophores. The two cell types are in different differentiation trajectories of neural crest cell through *pax7a*- and *pax7b*-dependent fate determination (Kimura et al. 2014). The *Dr* does not develop into tumor while *Sd* can progress into melanoma. This contrasts to the situation in the *mitf* promoter driven *xmrk* transgenic medaka, which develop several types of pigment cell tumors. In these fish the *xmrk* expression is driven by the *mitf* promoter that is active in xanthophores and melanophores. As a result, tumors formed in both cell lineages. Even so, the xanthophore tumor (i.e., xanthophoroma) only develops as epiphytic nodules without invasion. Xanthophoroma gene expression profile suggests it is less proliferative and less invasive than the melanoma counterpart (Sugiyama, Schartl, and Naruse 2019; Abdulsahib et al. 2023). The absence of the *xmrk* effect in xanthophores in *Xiphophorus* hybrids implies that despite *Sd* and *Dr* being linked, they are subjected to different regulation.

The genetics underpinning the *Dr* and *Sd* has not been resolved. Therefore, to study the discrepancy between *Sd* and *Dr*, we developed F₂ intercross interspecies hybrid between *X. maculatus* and *X. couchianus*. *X. maculatus* and *X. couchianus* are distantly related species. They are historically classified to southern and northern platyfish based on their habitat and phylogeny based on partial genome sequences (Kang et al. 2013). Morphologically, the two species are distinguished by body shape and pigmentation

patterns. Especially the *X. maculatus* has *Sd* and *Dr*, while *X. couchianus* does not possess either phenotype (Figure 1). Importantly, unlike the aforementioned *X. maculatus* and *X. hellerii* hybrid, *X. maculatus* and *X. couchianus* F₁ hybrid only exhibit *Dr*, but not *Sd*. Therefore, this hybrid offers a genetic model system that can be used to study diverged regulation of *Dr* and *Sd*. The *Dr* and *Sd* expressivity divergence leads to the hypothesis that *X. couchianus* genome encodes a dominant suppressor of *xmrk*-driven *Sd*. Given the phenotypic results from the F₁ hybrids, we tested whether *Sd* can express in F₂ interspecies hybrid population where a hypothetical dominant *X. couchianus* *xmrk* suppressor is conditionally lost, and subsequently investigated genetic mechanism underpinning of the *Sd* and *Dr*.

2 | Results

2.1 | Pigmentation Pattern Divergence in F₂ Interspecies Hybrids

In contrast to the analogous cross between *X. maculatus* (*Sd*+, *Dr*+) and *X. hellerii* (*Sd*–, *Dr*–), *Dr* is enhanced in *X. maculatus* and *X. couchianus* (*Sd*–, *Dr*–) F₁ interspecies hybrids (*mac-cou* hybrid) while *Sd* is not expressed in neither the *mac-cou* F₁

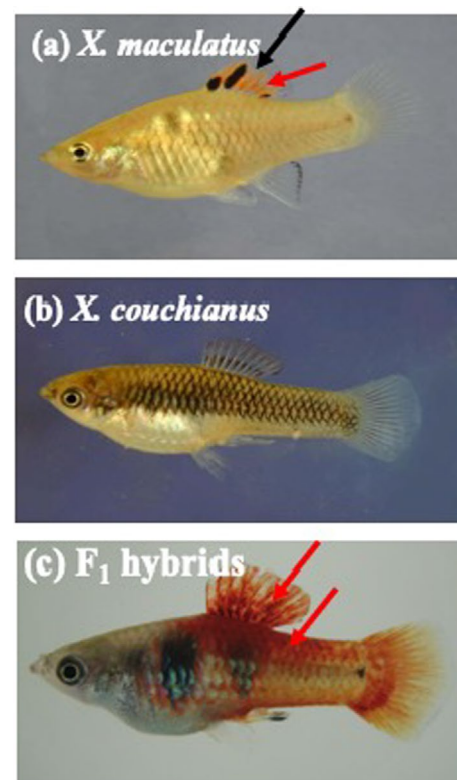


FIGURE 1 | Pigmentation patterns of *Xiphophorus maculatus*, *X. couchianus*, and their hybrid. (a) The *X. maculatus* exhibit a large dorsal fin spotting pattern that is encompassed by macromelanophore (*Spot Dorsal*, or *Sd*, pointed by black arrow). The dorsal fin also exhibits xanthophore-driven red coloration (*Dorsal Red*, or *Dr*, pointed by red arrow). (b) The *X. couchianus* does not exhibit *Sd* or *Dr*, but only background color made by micromelanophore. (c) The F₁ interspecies hybrids between the *X. maculatus* and *X. couchianus* display enhanced and expanded xanthophore pigmentation (pointed by red arrows), but not *Sd*.

nor backcross hybrid using *X. couchianus* as recurrent parent (Tables S1 and S2). We hypothesized that the *X. couchianus* genome encodes a dominant locus suppressing the *Sd* but not *Dr*. Therefore, we created a *mac-cou* F₂ interspecies hybrid population to assess *Sd* and *Dr* inheritance. We produced a total of 93 F₂ interspecies hybrids (*mac-cou* *hyb*). A 9.5% of the F₂ intercross hybrids exhibit *Sd*, compared to 64.8% expressed *Dr* (Table S3). All hybrids exhibiting *Sd* have *Dr*, but not vice versa.

We compared the skin gene expression profiles of the *mac-cou* *hyb* exhibiting *Sd* to the hybrids exhibiting only *Dr* and identified differentially expressed genes between the two pigmentation patterns. There are 28 genes over-expressed in *Sd*, including, as expected, genes related to the macromelanophore, melanocyte and melanoma (*slc24a5*, *st3gal3*, *st6galnac3*, *dct*, *oca2*, *melanopsin-A-like*, *fam19a1*, *tyrp1*, *pmel*, and *emilin2*). An unannotated gene, LOC11161040 that is the homolog to long neurotoxin OH-57 is the only gene under-expressed in *Sd* hybrids (Table 1).

2.2 | Segregation Between Two Oncogene-Driven Pigmentation Patterns in Interspecies Hybrids

We estimated interspecies variant sites' genotype and genetically mapped *Dr* and *Sd*. We categorized the F₂ population based on presence of *Dr* (*Dr+* and *Dr-*) or *Sd* (*Sd+* and *Sd-*). Mapping of *Dr* showed one single peak associated with the trait on chromosome (Chr) 21 between 24.27 to 25.03 Mbp. This region contains 18 gene models, including the *xmrk* (Figure 2a). All F₂ hybrids that are either homozygous for the *X. maculatus* alleles of genes within the peak region, or heterozygous for the peak region exhibited the *Dr* (Figure 2a; 100% penetrance).

In comparison, the *Sd* is associated with two loci, including a region located around 23.89 Mbp on Chr 21 that overlapped with one gene encoding an uncharacterized long noncoding RNA (Figure 2b), and another loci around 5.50 Mbp region on Chr13 that located between *long neurotoxin OH-57 like* and *sperm acrosome membrane-associated protein 4-like*. For the Chr21 locus, 20% of the *Sd* hybrids are homozygous for the *X. maculatus* allele, and 80% of the *Sd* hybrids are heterozygous for both parental alleles (Figure S2). In order to test if the Chr 21 loci underlying *Dr* and *Sd* are closely linked, we utilized a sub population of the F₂ hybrids that exhibited *Dr*, and categorized this population as *Dr+*, *Sd-* and *Dr+*, *Sd+*. The Chr21 loci became insignificant in associating with *Sd*, indicating the loci underpinning the *Sd* and *Dr* are not resolved (Figure S1).

The Chr 13 region associated with the *Sd* is preferentially, that is, 80% penetrance, homozygous for *X. maculatus* allele (Figure 3). All hybrid fish that exhibit *Sd* and are homozygous for *X. maculatus* allele showed extra macromelanophore pigmentation spots on trunk musculature. The two fish samples that exhibit *Sd* but are heterozygous for Chr13 (Fish 23), or homozygous for *X. couchianus* Chr13 (Fish 48) showed atypical *Sd* pigmentation pattern (Figure 3b,c). These melanophore clusters are smaller in size than those in *X. maculatus* parental. In addition, the macromelanophore distributed in a more dispersed pattern than the parental in which the macromelanophores aggregate to form a large spot (i.e., Figure 3c).

The definition of gene mapping relies on the total number of chromosome recombination. Therefore, we expected to observe that *Sd* hybrids would exhibit chromosomal recombination in loci that are adjacent to the Chr13 5.50 Mbp region. However, the chromosome recombination patterns showed by the haploid maps only support the shoulder region around the 5.50 Mbp peak (Figure 3, Figure S2). Similarly, recombination did not occur between Chr21 locus underlying *Dr* and the locus associated with *Sd* (Figure S2).

2.3 | Allelic Gene Expression Associated to *Dr* and *Sd*

For a gene to be functional, the minimum requirement is the expression of the allele underlying the function. We hypothesized that the alleles associated to *Sd* are preferentially expressed by one allele in *Sd-* as compared to *Sd+* hybrids. First of all, the *xmrk*, as a *X. maculatus* specific gene, showed the same level of *X. maculatus* allele specific expression in the hybrid expressing *Dr*, including the individuals that also display *Sd* (Figure S3). *Dr+* *Sd-* hybrids exhibited bi-allelic expression for *cdh6*, *droscha*, *mc4r*, and *cdh20*, while the hybrids without the *Dr* (*Dr-* *Sd-*) exhibit *X. couchianus* allele specific expression for *cdh6*, *droscha*, and *cdh20*, and no expression for *mc4r* (Figure 4a,b). These findings support that the *Dr* and *Sd* are *X. maculatus*-specific traits.

All *Sd+* hybrids exhibit *X. maculatus* allele specific expression for *long neurotoxin OH-57* and *sperm acrosome membrane-associated protein* (Figure 4c,d, Figure S3), but *X. couchianus* allele dominant expression for *long neurotoxin OH-57*, or bi-allelic expression for *sperm acrosome membrane-associated protein* in hybrids that do not exhibit *Sd* (Figure 4c,d). In addition, we surveyed the allelic expression patterns of all Chr 13 genes, *long neurotoxin OH-57*, and two additional genes (i.e., *fatty acid-binding protein 9-like* and *gastrula zinc finger protein XI CGF57.1-like*) that located on 6.38 and 6.63 Mbp regions are the only three genes exhibiting a *X. couchianus* allele dominant expression in *Dr+* *Sd-*, and *X. maculatus* allele dominant expression in *Dr+* *Sd+* hybrids (*X. maculatus*/*X. couchianus* <0.1 in *Dr+* *Sd-* hybrids and *X. maculatus*/*X. couchianus* >10 in *Dr+* *Sd+* hybrids, *p*-value <0.05; Figure 4e).

The *long neurotoxin OH-57* gene is the only gene that exhibited a lower expression in *Dr+* *Sd+* hybrids (Table 1), a genotype distribution bias from Hardy-Weinberg equilibrium (HWE), and reversed allelic expression patterns between *Dr+* *Sd-* and *Dr+* *Sd+* hybrids. The *X. maculatus* and *X. couchianus* *long neurotoxin OH-57* alleles exhibit two amino acid changes, A120T and G122S (Figure 5a). These two amino acids differences led to a shortened alpha-helix for the *X. couchianus* allele protein product and substitute a hydrophobic alanine for hydrophilic threonine (Figure 5b).

2.4 | Macromelanophore Can Be Modulated by Epinephrine Regulation

Melanosome trafficking is mediated by cAMP concentration (low cAMP triggers melanosome aggregation and high cAMP triggers melanosome dispersion). It was shown that

TABLE 1 | Differentially expressed genes between *Sd* and *Dr* hybrids skin.

Name	LogFC	LogCPM	<i>p</i>	FDR	Chr.number	Description
LOC102223073	1.73	0.96	0.0000	0.0004	1	RING finger protein 223-like%2C transcript variant X2
LOC102220729	1.22	1.48	0.0000	0.0001	1	Plexin-A1-like%2C transcript variant X1
slc35c2	0.55	6.17	0.0000	0.0012	1	Solute carrier family 35 member C2%2C transcript variant X4
LOC102233586	1.01	1.33	0.0000	0.0393	1	Voltage-dependent calcium channel subunit alpha-2/delta-3%2C transcript variant X1
slc24a5	1.61	0.76	0.0000	0.0000	4	Solute carrier family 24 member 5
st3gal3	1.06	5.07	0.0000	0.0120	6	ST3 beta-galactoside alpha-2%2C3-sialyltransferase 3%2C transcript variant X2
st6galnac5	1.85	0.09	0.0000	0.0061	6	ST6 N-acetylgalactosaminide alpha-2%2C6-sialyltransferase 5
st6galnac3	3.11	0.53	0.0000	0.0001	6	ST6 N-acetylgalactosaminide alpha-2%2C6-sialyltransferase 3
LOC102225053	1.98	1.79	0.0000	0.0003	7	Dehydrogenase/reductase SDR family member 13-like
dct	4.36	2.54	0.0000	0.0000	7	Dopachrome tautomerase
LOC111609588	2.88	-1.66	0.0000	0.0000	8	Uncharacterized LOC111609588
oca2	1.71	2.95	0.0000	0.0000	9	OCA2 melanosomal transmembrane protein
LOC102227481	2.34	-1.32	0.0000	0.0001	10	Melanopsin-A-like
kctd16	2.17	-0.03	0.0000	0.0291	11	Potassium channel tetramerization domain containing 16%2C transcript variant X1
LOC102232444	1.35	2.03	0.0000	0.0001	12	Sia-alpha-2%2C3-Gal-beta-1%2C4-GlcNAc-R:alpha 2%2C8-sialyltransferase-like
grid2	2.46	2.94	0.0000	0.0323	12	Glutamate ionotropic receptor delta type subunit 2%2C transcript variant X1
LOC111610400	-2.66	1.76	0.0000	0.0106	13	Long neurotoxin OH-57-like
tyrp1	1.15	5.26	0.0000	0.0001	14	Tyrosinase-related protein 1
LOC102223628	3.15	1.06	0.0000	0.0422	14	Uncharacterized LOC102223628
LOC111611782	2.45	4.45	0.0000	0.0044	17	Uncharacterized LOC111611782%2C transcript variant X2
slc26a3	3.35	3.53	0.0000	0.0089	17	Solute carrier family 26 member 3

(Continues)

TABLE 1 | (Continued)

Name	LogFC	LogCPM	<i>p</i>	FDR	Chr.number	Description
LOC102223560	1.68	5.50	0.0000	0.0000	20	Melanocyte protein PMEL%2C transcript variant X1
LOC102230798	2.00	2.15	0.0000	0.0302	20	Protein FAM19A1-like%2C transcript variant X3
emilin2	1.47	6.02	0.0000	0.0004	21	Elastin microfibril interfacier 2
LOC102238269	1.60	1.61	0.0000	0.0008	22	Stromal membrane-associated protein 1%2C transcript variant X1
ercc6	1.40	6.19	0.0000	0.0000	22	ERCC excision repair 6%2C chromatin remodeling factor
LOC102223853	1.89	-0.44	0.0000	0.0001	22	Dorsal root ganglia homeobox protein-like
LOC102228648	2.42	-0.09	0.0000	0.0003	22	Carbonyl reductase [NADPH] 1-like%2C transcript variant X1
glra1	1.82	-0.83	0.0000	0.0269	23	Glycine receptor alpha 1%2C transcript variant X6

melanosomes aggregate following epinephrine exposure in *Gambusia holbrooki* melanophores. As we showed that a *long neurotoxin OH-57* is involved in the macromelanophore patterning, we hypothesized that *Xiphophorus* macromelanophore is subjected to neuronal regulation. We treated *Xiphophorus* fish with macromelanophores patterns, including *X. xiphidium* and F₁ hybrid between *X. maculatus* and *X. couchianus* with 2.4 mg/mL epinephrine. Macromelanophores exhibited melanosome aggregation following 5 and 10 min of epinephrine treatment in *X. xiphidium* (Figure 6a) and *X. maculatus*-*X. couchianus* hybrids (Figure 6b) respectively.

3 | Discussion

In this study, we identified the long-sought loci underlying an ornamental trait *Dorsal red (Dr)* and disease-related trait, *Spotted dorsal (Sd)* in *Xiphophorus* fish (Meyer, Morrissey, and Schartl 1994).

Our finding showed the *Dr* is a *X. maculatus* monogenic dominant trait with 100% genetic penetrance. This is well supported by our breeding records of hybrids involving *X. maculatus*, which display *Dr*, and from observations that phenotypical distribution of *Dr* follows a pattern that is consistent with expectations from a single dominant locus (Tables S1 and S2, Figure 2a). It is important to note that *Dr* is a xanthophore pigmentation pattern and should be distinguished from the *xmrk* gene. The *xmrk* gene is a driver for cellular proliferation (Monroe, Basheer, and Gibert 2021; Zheng et al. 2014; Schartl et al. 2010; Wellbrock et al. 2002; Wellbrock, Fischer, and Schartl 1998), while the *Dr* locus serves compartmentalization function that determines the spatial expression pattern of *xmrk*. In this regard, the cadherin genes (*cdh6* and *cdh20*) within the *Dr* locus are strong candidate genes accounting for the *Dr* phenotype.

Second, the loci underlying *Sd* and *Dr* are proximate on the *X. maculatus* sex chromosome Chr 21 but are regulated differently. The *Sd* and *Dr* pigmentation patterns are always linked in hybrids between *X. maculatus* and *X. hellerii* (Lu, Sandoval, et al. 2020; Lu, Olivas, et al. 2020), and were thus thought to be regulated simultaneously. In this study, *Dr* and *Sd* are mapped to the same region on Chr 21. This observation supports the initial thought that *Sd* and *Dr* are physically linked. However, unexpectedly, we showed that despite loci underlying *Dr* and *Sd* being proximate to each other, the two traits are not necessarily co-regulated, as hybrids between *X. maculatus* and *X. couchianus* can display *Dr* independent of *Sd*. The finding that low expression of an autosomal locus from the *X. maculatus* (Chr 13) is needed for *Sd* expression suggests that *X. couchianus* allele of the locus can suppress *Sd*. We found that *long neurotoxin OH-57* gene is a candidate gene for regulating the *Sd*, evidenced by its *X. maculatus* allele-specific low expression in *Sd+* hybrids, and the expression of *X. couchianus* allele in *Sd-* hybrids. However, the suppression of *Sd* is likely mediated by more than the *long neurotoxin OH-57* locus, as *Sd* is observed in only 10% of the F₂ hybrids, which is lower than an otherwise expected 25% for two-loci interaction, and the presence of 6 *Dr+* *Sd-* hybrids that showed lowly expressed *X. maculatus* allele-only expression for this gene. The *Sd* phenotype exhibition is known to vary with age. Even an isogenic population can display this phenotype at different ages. Since all F₂ hybrids were euthanized for sample collection at 9-month-old, the discrepancy in percentage of observed *Sd+* hybrid and anticipated *Sd+* hybrid from a two-gene model can also be sourced to a delayed development of *Sd*. However, from preliminary observations of aged F₂ hybrid population (20 months old and above), delayed *Sd* development has not been observed. Taken the *Sd* and *Dr* genetic mapping results together, we conclude *Sd* and *Dr* are two cell type-specific regulatory sequences for *xmrk*, with *Sd* for macromelanophore lineage, and *Dr* for xanthophore lineage (Figure 7).

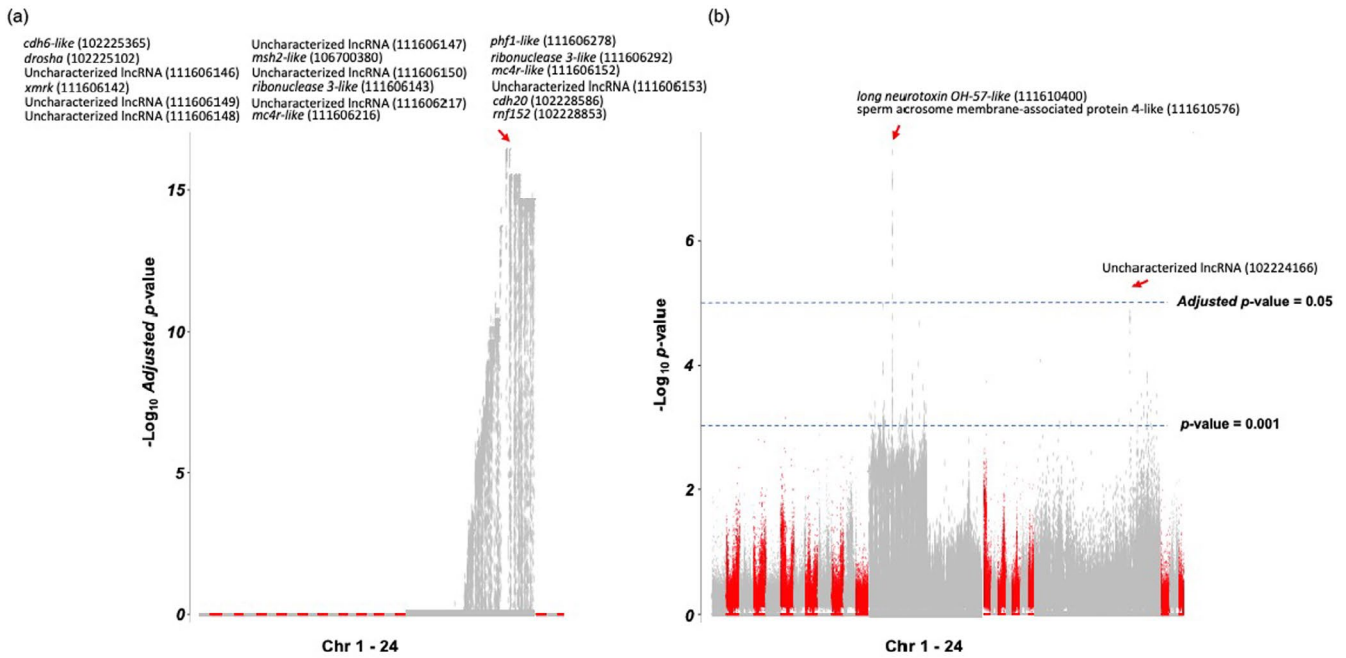


FIGURE 2 | Genetic mapping identifies one locus underlying *Dr* and two loci underlying *Sd*. Interspecies hybrids were produced by mating male and female *Xiphophorus maculatus*–*X. couchianus* F₁ hybrids. (a) Genetic mapping showed one single peak on Chr 21 is associated to the *Dr*. In the Manhattan plot, X-axis represent all 24 chromosomes, with gray represented odd number chromosomes and red represented even number chromosome. Non-Chr 21 chromosomes were reduced in size as there is no statistically significant locus identified on them. Y-axis represent multiple test correction adjusted *p*-values that are transformed to $-\log_{10}$ Adjusted *p*-value. The *Dr* is mapped to 24.27 to 25.03 Mbp on Chr 21. This region contains 18 genes. All *Sd*+ F₂ hybrids are either homozygous for the *X. maculatus* allele, or heterozygous for both parental alleles in the peak region. (b) The *Sd* is mapped to a region around 5.50 Mbp region on Chr 13 and 23.89 Mbp region on the Chr 21. The Chr 13 region contains two genes, and the Chr 21 region contains one gene. For the Chr 13 locus, 80% of the *Sd*+ hybrids are homozygous for the *X. maculatus* allele, 20% are either homozygous for *X. couchianus* allele, or heterozygous for both parental alleles. For the Chr 21 locus, 20% of the *Sd* hybrid is homozygous for *X. maculatus* allele, and 80% of the *Sd* hybrid is heterozygous for both parental alleles. *Dorsal red*, or *Dr*, is pointed by red arrow.

The *Sd* pattern is known to be driven by *xmrk* oncogene. Genes suppressing the *xmrk* function have been found from several genetic mapping studies utilizing hybrids between *xmrk* positive and negative species. These regulators include *myrip* and *adgre5* in *X. malinche*–*X. birchmanni* hybrids, *cdkn2ab* and *rab3d* in *X. maculatus*–*X. hellerii* hybrids (Lu, Sandoval, et al. 2020; Lu et al. 2017; Powell et al. 2020; Kazianis et al. 1998; Nairn et al. 1996). In all cases, segregation between *xmrk* and the functional alleles of the regulators leads to lethal melanoma. Therefore, these regulators were interpreted as co-evolved with the *xmrk* oncogene to fine-tune the activity of it and suppress its oncogenic function. The negative epistasis between *xmrk* and nonfunctional alleles of these regulators in varied *Xiphophorus* hybrids serve as evidence supporting the Dobzhansky–Muller hybrid incompatibility model that states negative epistatic interactions occurring between genes that are adaptive in different species account for hybrid incompatibility and act as a post-zygotic barrier shielding gene flow between different species. However, in this study, *long neurotoxin OH-57-like* allele of *X. couchianus*, a species that does not have *xmrk*, fully “suppresses” the *xmrk*-driven *Sd* phenotype from a different species. The apparent “suppression” of *Sd* can be interpreted as either inhibition or lack of enhancement of *Sd* by *X. couchianus* allele than the *X. maculatus* allele. Macromelanophore pigmentation patterns, including *Sd*, are sexually selected [for review, see (Tanja and Zerulla 2021)], such that presenting it at an adequate level is favored by sexual selection despite uncontrolled

upregulation of *xmrk* is deleterious (i.e., melanoma). In this respect, the *X. maculatus* allele of *long neurotoxin OH-57* is a *xmrk* regulator that co-evolved with *xmrk*, by enhancing the *Sd* pigmentation. The *xmrk* originated from a local *egfr* gene duplication event. Multiple *Xiphophorus* species have it. A recent *Xiphophorus* phylogeny indicates that *X. couchianus* ancestral species lost the *xmrk* gene (Du et al. 2024). When *xmrk* was lost, the *X. couchianus long neurotoxin OH-57-like* could degenerate due to no purification co-selection (Figure S4).

Expansion and enhancement of macromelanophore pigmentation patterns in *Xiphophorus* are linked to the *xmrk* activity. A macromelanophore is characterized by its large size and is multinucleated (Regneri et al. 2019). The *xmrk* gene and a hypothetical locus tightly linked to *xmrk* are thought to control the proliferation and compartmentalization of macromelanophore, respectively. For instance, a different laboratory strain *X. maculatus* (i.e., *X. maculatus* Jp163B) are fixed for *Spot Side (Sp)*, a different allele of macromelanophore patterning locus than *Sd*, exhibits macromelanophore on the body side (Lu, Olivas, et al. 2020). In order for macromelanophore to be functional, several conditions are required: (1) differentiation of macromelanophore from melanoblast; (2) functional melanin synthesis pathway; (3) assembly of melanosome; (4) microtubule for melanosome transportation; and (5) intact signaling cascade regulating melanosome aggregation and dispersion within melanophore (Figure 7). The *xmrk* drives macromelanophore proliferation

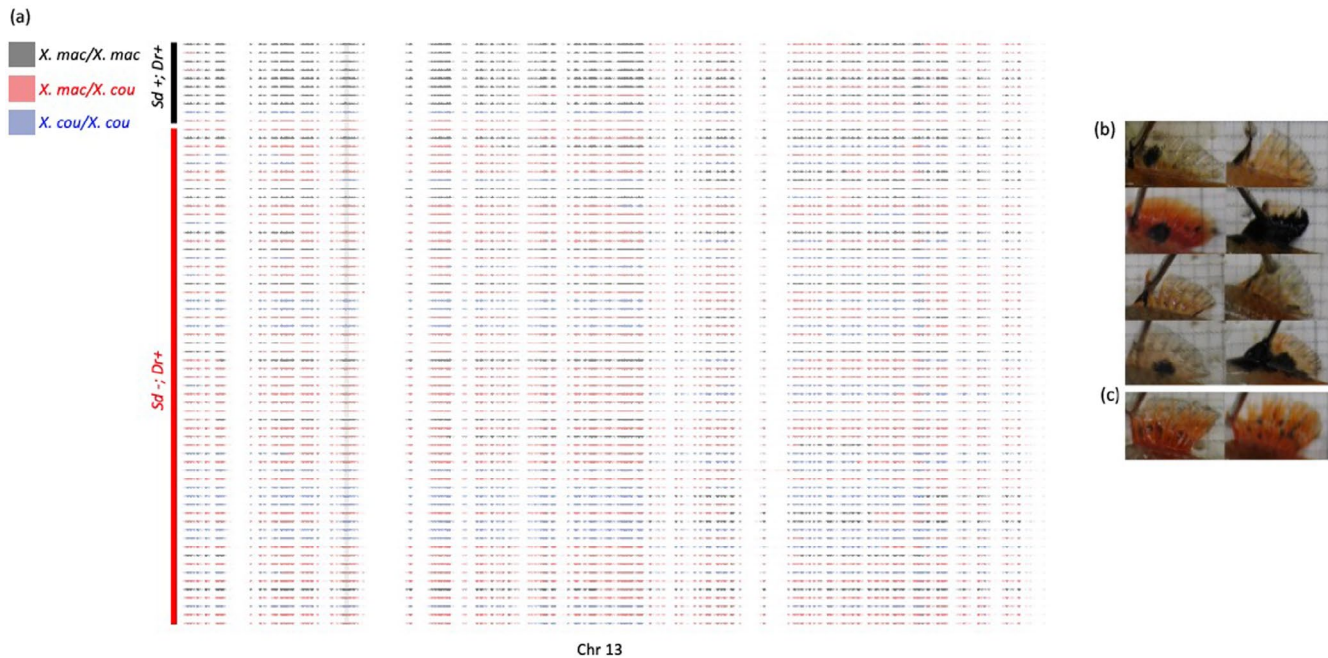


FIGURE 3 | Chromosome recombination pattern does not support genetic segregation between *Sd* and *Dr*. (a) Haploid map for Chr 13 for *Dr+* *Sd-* and *Dr+* *Sd+* hybrids were made by plotting genotype of inter-specific polymorphism genotypes along their chromosomal coordinates. Gray, red, and blue dots are respectively polymorphic sites that are homozygous for *Xiphophorus maculatus*, heterozygous for both parental alleles, and homozygous for the *X. couchianus* allele. Chromosomal recombination took place where bars of different colors meet. Vertical shaded gray line marks loci underlying *Sd*. (b) The melanophore patterns for 8 *Sd+* hybrids. (c) The melanophore patterns for two *Sd+* hybrids that exhibited irregular macromelanophore patterns. They are characterized by smaller melanophore aggregates and more dispersed micromelanophore pattern that is distributed between fin rays.

(Wellbrock et al. 2002; Wellbrock, Fischer, and Schartl 1998; Morcinek et al. 2002). Several genes have been found to regulate *xmrk* oncogenicity using interspecies hybrids involving species encoding *xmrk*. These include genes that are thought to directly interact with melanosome assembly and transportation *rab3d* and *myrip* (Lu, Sandoval, et al. 2020; Lu et al. 2017; Powell et al. 2020). Additional regulators include cell cycle regulator *cdkn2ab* (Lu et al. 2017; Kazianis et al. 1998; Nairn et al. 1996), and cell adhesion, invasion-related gene *adgre5* (Powell et al. 2020). The current finding that the *xmrk*-driven macromelanophore presentation is reliant on allele-specific expression of a neurotransmission regulator gene (i.e., *long neurotoxin OH-57-like*) suggests that the presentation of macromelanophore pattern has an additional point of regulation that is subjected to epistatic interactions. It has been shown that melanophores can be regulated by neuronal or hormonal ligands (Regneri et al. 2019; Kottler et al. 2020). We have also shown that macromelanophore is regulated by adrenergic receptor signaling, despite the adrenaline-induced melanosome aggregation is not complete as observed in micromelanophore. From the understanding of how long neurotoxin Oh-57 work, that is, binding to nicotinic acetylcholine receptor (nAChR) and inhibits acetylcholine from binding to nAChR (He, Lee, and Zhang 2004), the *long neurotoxin OH-57-like* is likely to be a neurotransmitter receptor regulator in *Xiphophorus*. Our simulated *Xiphophorus* long neurotoxin OH-5-like peptide binding to nAChR is consistent with experimental solved neurotoxin-nAChR binding structure in terms of binding site and conformation (Figure S5). Collectively, this newly identified *xmrk* regulatory point is likely due to incompatibility

between macromelanophore and neurotransmitter regulator between different species.

In conclusion, we have identified a locus underlying a sex chromosome linked ornamental trait that is tightly linked to an oncogene in the *Xiphophorus*. Despite physical proximity, the ornamental trait loci and the oncogene are subjected to different genetic regulation by an autosomal regulator.

4 | Materials and Methods

4.1 | Animals

Xiphophorus maculatus, *X. couchianus*, first-generation (F_1) interspecies hybrids between *X. maculatus* and *X. couchianus*, and intercross hybrids between F_1 hybrids used in this study were supplied by the *Xiphophorus* Genetic Stock (<http://www.xiphophorus.txstate.edu/>). The F_1 interspecies hybrids between *X. maculatus* Jp163A strain fish and *X. couchianus* were produced by enforced mating, and F_2 hybrids were produced naturally by F_1 hybrids. All fish were kept and samples taken in accordance with protocols approved by Texas State University IACUC (IACUC9048). All fish were dissected at age of 9 months. At dissection, all fish were anesthetized in an ice bath and upon loss of gill movement sacrificed by cranial resection. Dorsal fin clips were dissected and preserved in ethanol. Organs were dissected into RNAlater (Ambion Inc.) and kept at -80°C until use.

4.2 | Phenotyping

Two pigmentation patterns, the macromelanophore pattern *spot dorsal*, and xanthophore pattern *dorsal red*, were typed. Before dissection, fish were nailed to a grading paper by using dissection needles to stabilize dorsal fin and anal fin. The *spot dorsal*

is determined by a large black pigmented spot on the dorsal fin. This spotting pattern is different from the common micromelanophore pattern that is observed in all *Xiphophorus* fishes, which is smaller in size and distributed between fin rays on the dorsal fin. The *dorsal red* is determined by red coloration on the dorsal fin. The phenotyping results were agreed by four independent typing.

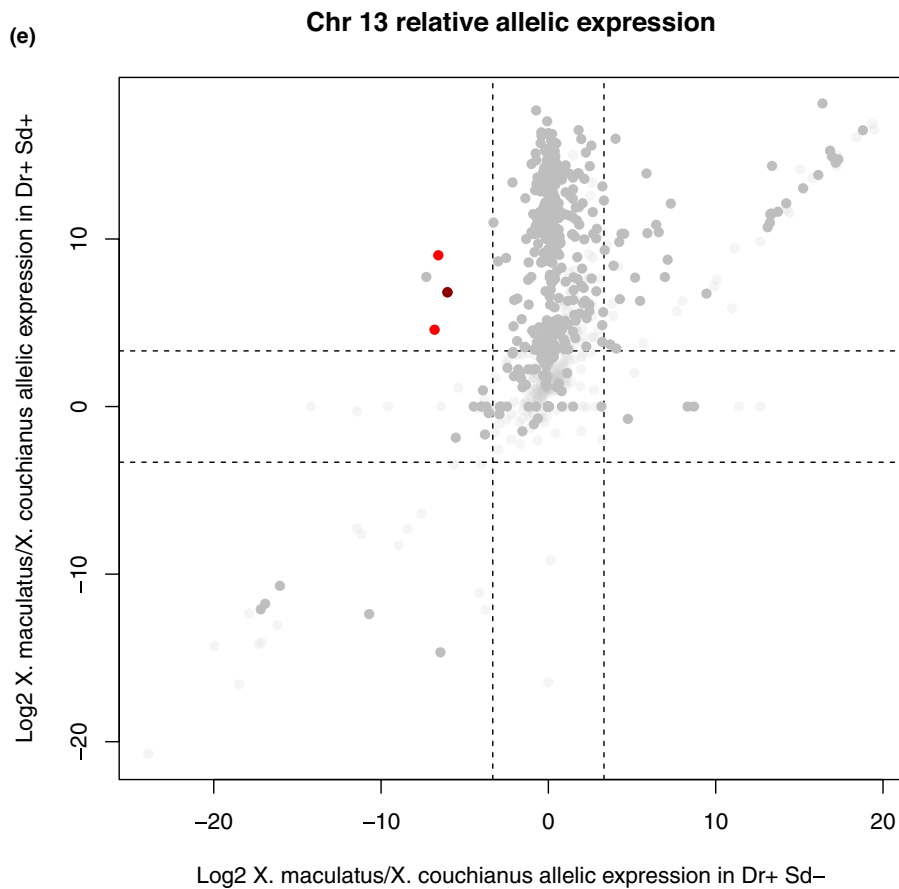
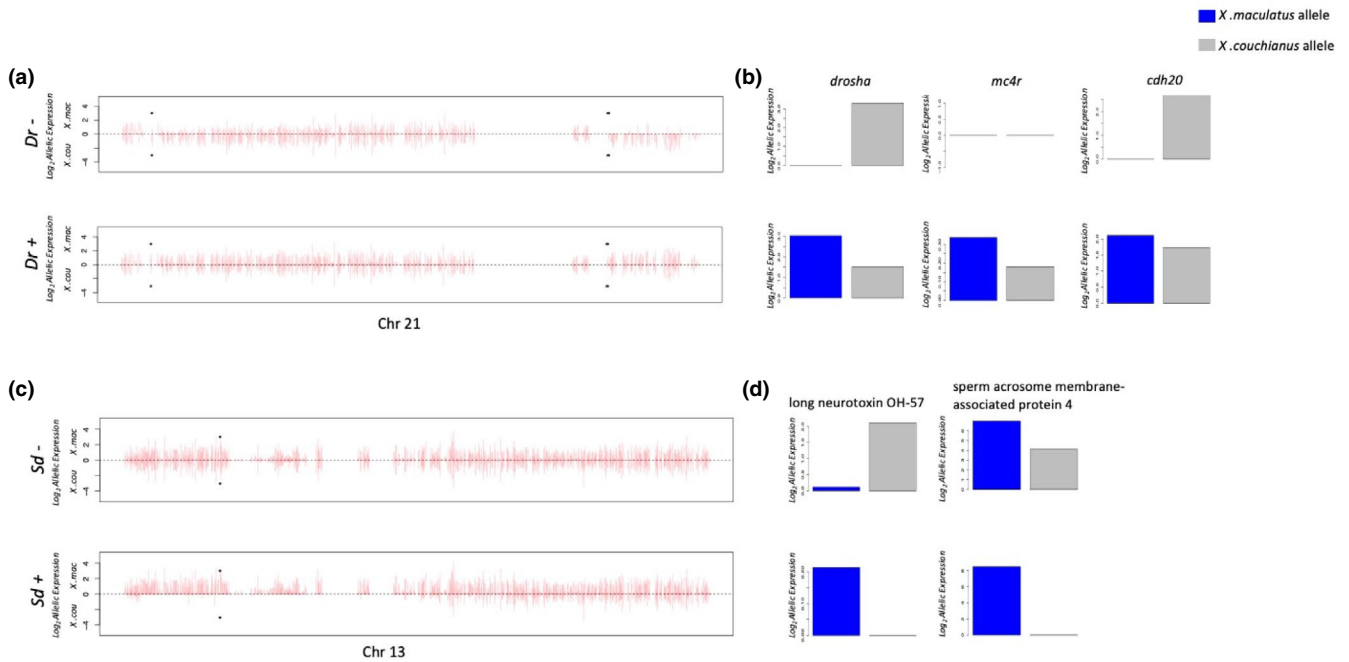


FIGURE 4 | Allelic gene expression pattern hallmarks genes associated with *Dr* and *Sd*. (a) The upper panel and lower panel shows allelic expression in *Dr*⁻ and *Dr*⁺ hybrids respectively. Allelic expression values were normalized. Bars above the middle line represent the *Xiphophorus maculatus* alleles, and bars under the middle line represent *X. couchianus* alleles. Bars are plotted in the order of *X. maculatus* gene orders on Chr 21. Asterisks hallmark positions of candidate gene models. Because the Chr 21 assembly has a double-inversion assembly error, the candidate genes locate distantly while in a corrected assembly are next to each other. (b) Bar graphs show candidate gene specific allelic expression patterns. The blue bars represent the *X. maculatus* allele, and gray bars represent the *X. couchianus* allele. (c) The upper panel and lower panel shows allelic expression in *Sd*⁻ and *Sd*⁺ hybrids respectively. Bar heights represent allelic expression levels as in (d), and bars are plotted in the order of *X. maculatus* gene orders on Chr 13. Asterisks hallmark positions of candidate gene models. For alleles that are not expressed, they were assigned a 0 value for (b) and (d). (e) Dot plots show relative allelic expression of Chr 13 genes in *Dr*⁺ *Sd*⁻ and *Dr*⁺ *Sd*⁺ hybrids. For each dot, the X-coordinate represent relative expression levels of *X. maculatus* over *X. couchianus* alleles in *Dr*⁺ *Sd*⁻ hybrids, and the Y-coordinate represent relative expression levels of *X. maculatus* over *X. couchianus* alleles in *Dr*⁺ *Sd*⁺ hybrids. The dashed lines that located at Log₂0.1 and Log₂10 that correspond to relative expression ratio of 0.1 or 10 separates the graphs in nine regions. Dots in the top left and bottom right regions represent genes that dominantly expressed for one allele in *Sd*⁻ hybrids but the other allele in *Sd*⁺ hybrids. Light gray dots are all genes on the Chr 13, with dark gray dots highlighted all genes in the Figure 2 Manhattan plot shoulder region. Red dots highlighted genes exhibit reversed dominant allelic expression between *Sd*⁻ and *Sd*⁺ hybrids. The dark red spot highlighted *long neurotoxin OH57* like. Allelic gene expression patterns for Chr 21 and Chr 13, and genes underlying *Sd* and *Dr* candidate regions are shown.

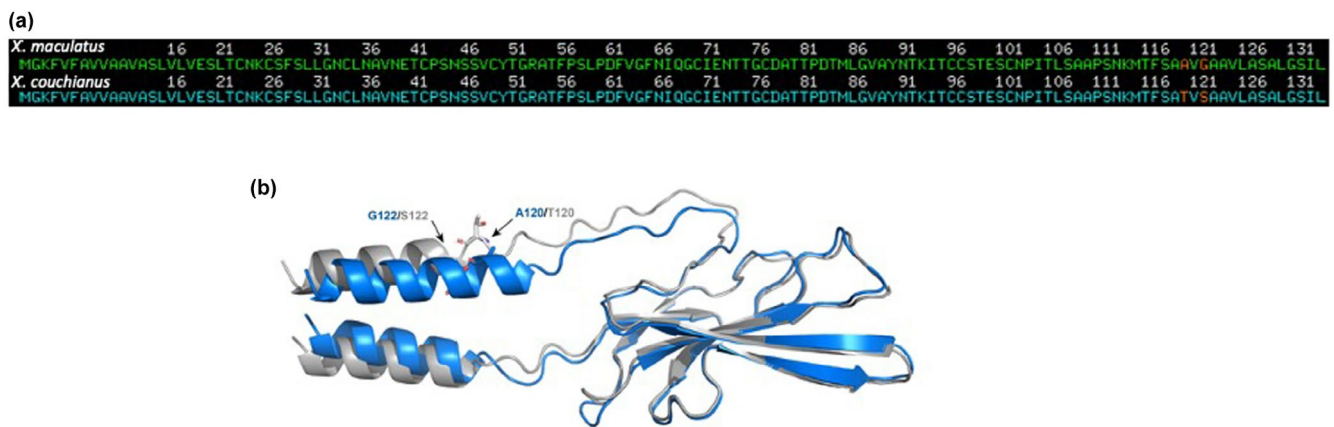


FIGURE 5 | Structural comparison between *Xiphophorus maculatus* and *X. couchianus* alleles for long neurotoxin OH-57-like peptide. (a) Primary peptide sequences comparison between the *X. maculatus* and *X. couchianus* alleles of long neurotoxin OH-57-like exhibit two amino acid changes (b) Structural alignments of long neurotoxin OH-57-like peptides derived from *X. maculatus* (blue) and *X. couchianus* (grey) using the align function of PyMOL.

4.3 | DNA and RNA Isolation

Fin clip of four *X. maculatus* males and five *X. couchianus* males were collected and digested by Protease K at room temperature for 1 h. The lysate was then transferred to 2.0 mL collection tubes. DNA isolation was performed by a QIAcube HT (Qiagen) automated bio-sample isolation system, with reagent contained in QIAamp 96 DNA QIAcube HT Kit. The isolation system is equipped with a robotic arm with eight pipettes. Each pipette is able to pick and eject pipette tips, self-clean, and transfer liquids between wells/columns, or between master reservoirs and wells/columns in standard 96-well plate formats. Each sample was independently maintained throughout the isolation process. Concentrations of DNA samples were measured using Qubit 2.0 fluorometer (Life Technologies, Grand Island, NY, USA), and adjusted for sequencing library preparation. Skin samples were homogenized in TRI-reagent (Sigma Inc., St. Louis, MO, USA) followed by addition of 200 μ L/mL chloroform, vigorously shaken, and subjected to centrifugation at 12,000 g for 5 min at 4°C. Total RNA was further purified using an RNeasy mini RNA isolation kit (Qiagen, Valencia, CA, USA). Column DNase

digestion at 25°C for 15 min removed residual DNA. Total RNA concentration was determined using a Qubit 2.0 fluorometer (Life Technologies, Grand Island, NY, USA). RNA quality was verified on an Agilent 2100 Bioanalyzer (Agilent Technologies, Santa Clara, CA, USA) to confirm that RIN scores were above 7.0 prior to subsequent gene expression profiling.

4.4 | Inter-Specific Genetic Variants Identification and Annotation

To identify interspecies polymorphisms between the *X. maculatus* and *X. couchianus*, genomic DNAs of four *X. maculatus* and five *X. couchianus* were isolated and forwarded for genome shotgun sequencing library preparation using Illumina Nextera sequencing Library Prep Kit, followed by sequencing on HiSeq 2000 (Illumina, Inc., San Diego, CA, USA) using 150 bp paired-end (PE) sequencing strategy. Raw sequencing reads were filtered using fastx_toolkit (http://hannonlab.cshl.edu/fastx_toolkit/index.html). Filtered sequencing reads were mapped to the reference *X. maculatus* genome (GenBank assembly

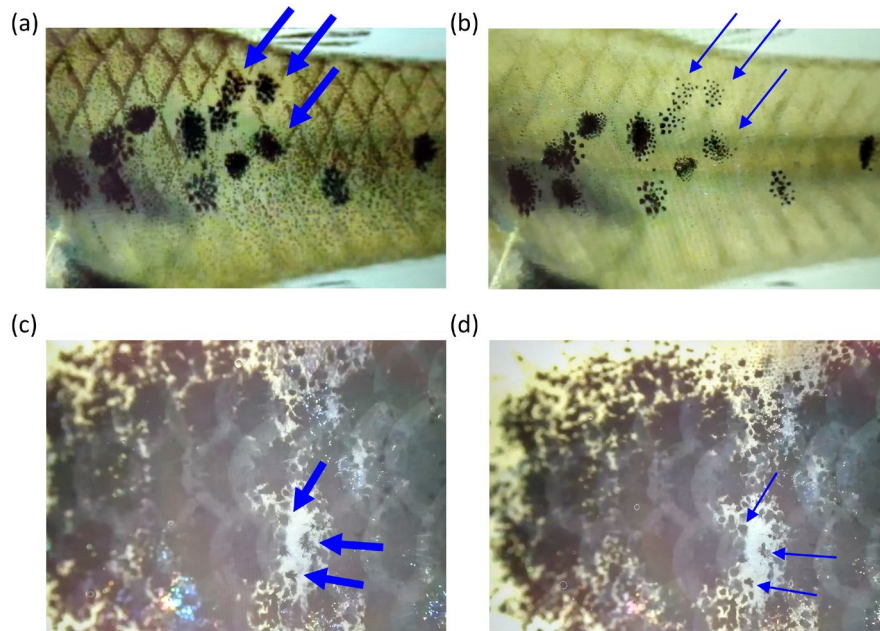


FIGURE 6 | Epinephrine treatment triggers melanosome aggregation in macromelanophore. Epinephrine (24 mg/mL) were treated to *Xiphophorus xiphidium* (a, b), and interspecies hybrid between *X. maculatus* and *X. couchianus* (c, d). (a) Before treatment, (b) 5 min after treatment, (c) before treatment, and (d) 10 min after treatment. Thick blue arrows indicate pre-epinephrine treatment macromelanophore, and thin blue arrows indicate post-epinephrine treatment mecaomelanophore.

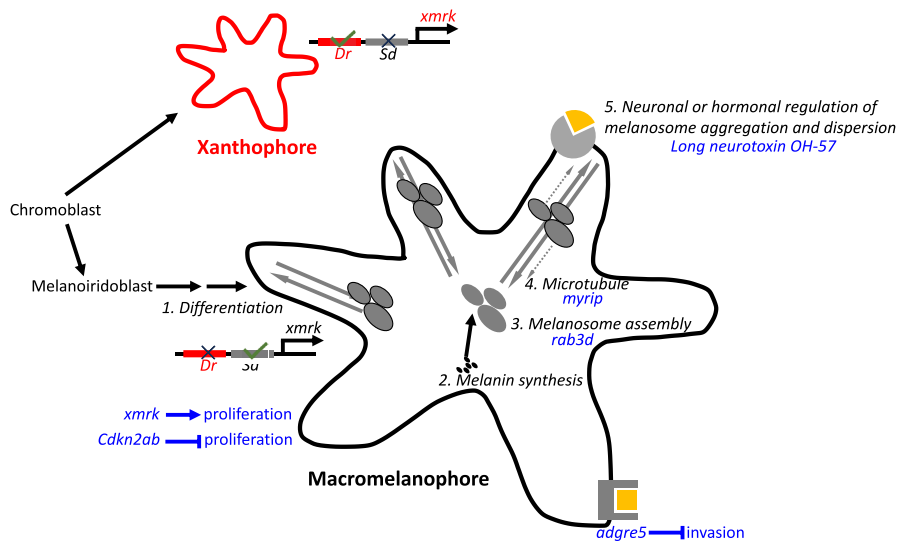


FIGURE 7 | Overview of *xmrk* and regulator activity.

accession: GCA_002775205.2) using Bowtie2 “head-to-head” mode (Langmead and Salzberg 2012). Alignment files were sorted using Samtools (Li et al. 2009). Pileup files were generated for each *X. maculatus*, and *X. couchianus* sample, and variant calling was processed by BCFtools for polymorphisms detection, with minimum variant locus coverage of 2 and variant genotyping call Phred score of 0 and alternative genotyping Phred score ≥ 20 for BCFtools (Li et al. 2009; Li 2011; Koboldt et al. 2009). Genotype refers to inheritance of ancestral alleles, with heterozygous meaning that a locus exhibited genetic material from both ancestors (i.e., *X. maculatus* and *X. couchianus*), and homozygous means that a locus exhibited genetic material from only one parental species. Inter-specific polymorphic sites where all sequenced *X. maculatus* support a homozygous

X. maculatus reference, and *X. couchianus* support a homozygous alternative variant calls were kept as a reference of genetic variance in .bed format.

4.5 | Gene Expression Profiling and Allelic Expression Profiling

RNA sequencing was performed upon libraries constructed using the NEB stranded mRNA-seq library preparation kit (New England Biolabs, Ipswich, MA, USA). RNA libraries were sequenced as 150 bp pair-end fragments using Illumina Novaseq system (Illumina, Inc.). RNA libraries were sequenced as 150 bp paired-end fragments using Illumina NovaSeq system (Illumina,

Inc.). Short sequencing reads were filtered using `fastx_toolkit` (http://hannonlab.cshl.edu/fastx_toolkit/contact.html). RNA-Seq sequencing reads were produced from independent skin samples of F_2 hybrids exhibiting *Sd* and only *Dr*. Sequencing reads were mapped to *X. maculatus* reference genome (GenBank assembly accession: GCA_002775205.2) using Tophat2 (Kim et al. 2013; Lu et al. 2023). Gene expression was subsequently profiled by counting number of sequencing reads that mapped to gene models annotated by NCBI using Subread package FeatureCount function (Liao, Smyth, and Shi 2013). Differentially expressed genes were identified using R package edgeR, with p -value adjusted using false discovery rate (FDR) method (Robinson, McCarthy, and Smyth 2010). $|\text{Log}_2\text{FC}| > 1$ and $\text{FDR} < 0.05$ was used to determine differentially expressed genes.

We used an established method to assess allelic expression of the F_2 hybrids (Lu et al. 2021). Briefly, orthologs between the parental alleles were identified using `blastn`, with the *X. maculatus* transcripts as subject and *X. couchianus* as reference. Both parental alleles were subsequently combined to represent a hybrid transcriptome. RNA-Seq reads were mapped to this hybrid transcriptome using Bowtie2 (Langmead and Salzberg 2012), followed by filtering of the read mapping file to keep reads that were mapped uniquely to one allele, and quantification of these reads per allele. Both parental alleles read counts of a gene was normalized to the length of parental allele lengths and were used to estimate percentages of gene expression contributed by either parental allele. These ratios were subsequently used to calculate allele expression using the library size normalized total read counts. Allelic expression differences were tested using R package edgeR, with p -value adjusted using FDR method (Robinson, McCarthy, and Smyth 2010). $|\text{Log}_2\text{FC}| > 1$ and $\text{FDR} < 0.05$. For data visualization, gene expression read counts were normalized to library size and were plotted as bar graph using custom scripts in R (v3.5.1).

4.6 | Genome Mapping of *Spot Dorsal* and *Dorsal Red*

Sequencing adaptor contamination of RNA-Seq reads was first removed from raw sequencing reads using `fastx_toolkit`, followed by trimming of low-quality sections of each sequencing read. Low-quality sequencing reads were further removed from sequencing result (http://hannonlab.cshl.edu/fastx_toolkit/index.html). Processed sequencing reads were mapped to *X. maculatus* genome v5.0 (GenBank assembly accession: GCA_002775205.2) using Bowtie2 (Langmead and Salzberg 2012). Mpileup files were made using legend version of samtools (v0.19) and genotyping was processed using Bcftools. Genotype in this study refers to inheritance of ancestral alleles, with heterozygous meaning that a locus exhibited genetic material from both ancestors (i.e., *X. maculatus* and *X. couchianus*), and homozygous means that a locus exhibited genetic material from only the one parental species. This samtools version performs ChiSq test for genotyping distribution against Hardy Weinberg Equilibrium between two groups. Hybrid individuals that do not exhibit phenotype-to-test were assigned as group 0 and individuals that exhibit a phenotype were assigned as group 1. The ChiSq test p -values

were adjusted using Bonferroni method, and were converted to $-10 \times \text{Log}_{10} p$ -value for Manhattan plot. To assess individual genotype at reference inter-specific polymorphic sites, genotype calls were required to be supported by specific statistics (i.e., Bcftools: $\text{MAPQ} \geq 30$, Phred score of genotype call = 0, with alternative genotype call Phred score ≥ 20).

4.7 | Protein Structural Simulation

The primary amino acid sequences of long neurotoxin OH-57-like peptide for *X. maculatus* (XP_023200269.1) and *X. couchianus* (XP_027891100.1) were retrieved from NCBI. The structural models of long neurotoxin OH-57-like peptides were obtained from the protein structural prediction software, ColabFold (Langmead and Salzberg 2012). ColabFold combines the homology search of Many-against-Many sequence searching (MMseqs2) (Steinegger and Soding 2017) with AlphaFold2 (Jumper et al. 2021) to predict protein structures and complexes. For each peptide, five models were generated and the model with the highest mean pLDDT score—76.72 for *X. couchianus* and 76.80 for *X. maculatus*—was selected for alignment. The chosen models were then aligned and visualized using PyMOL, focusing on structural variations.

4.8 | Protein Docking and Visualization

The initial structure of the nicotinic acetylcholine receptor (nAChR) was obtained from the protein data bank (PDB), specific as 2BG9. Only the extracellular region of the nAChR was used in the following docking process. The docking study to investigate the interaction between the long neurotoxin OH-57-like peptide, which obtained from ColabFold, and the extracellular region of nAChR was conducted using the ZDOCK (<https://zdock.wenglab.org>) and ZRANK programs. Initially, ZDOCK was employed to predict potential binding poses of the peptide to the receptor. ZDOCK utilizes a fast Fourier transform (FFT) algorithm to perform a comprehensive search of the rotational and translational space between the receptor and ligand, generating a set of possible docked conformations (Pierce, Hourai, and Weng 2011). Following the initial docking, the top-ranked poses from ZDOCK were further refined using ZRANK. ZRANK re-ranks the docking poses based on a detailed scoring function that considers additional energy terms, including van der Waals, electrostatics, and desolvation contributions (Pierce and Weng 2007). This refinement step ensures a more accurate prediction of the binding affinity and interaction specifics. The docking structure was visualized using PyMOL.

4.9 | Epinephrin Treatment to *Xiphophorus*

Two types of *Xiphophorus* fish exhibiting macromelanophore pigmentation patterns, *X. xiphidium* (RP line) and F_1 interspecies hybrid between *X. maculatus* (Jp163B) and *X. couchianus*, were provided by the *Xiphophorus* Genetic Stock Center. Fish were euthanized by over-dosing MS222. Following loss of gill movement, fish were decapitalized and immersed in 24 mg/mL Epinephrin (Fisher Scientific, Hampton, NH). Macromelanophores were videotaped for 10 min.

4.10 | Inter-Species Chromosomal Orthologous Region Identification

To identify genome region of *X. couchianus* that is orthologous to *X. maculatus* region underlying candidate *Dr* locus, we used LiftOff (<https://github.com/agshumate/LiftOff>) to map *X. maculatus* genes onto *X. couchianus*. After synteny filtering, we found genes within a ~200 kb area of *X. maculatus* chr21 failed to map onto *X. couchianus*, including *xmrk*. To further confirm this synteny gap, we used minimap2 (Li 2018, 2021) to align the whole genome between the two species and improved the alignment with Genome Alignment Tools from the Hiller lab (Osipova, Hecker, and Hiller 2019; Suarez et al. 2017).

Acknowledgments

This work was supported by the National Institutes of Health, National Cancer Institute, R15 CA-223964 to Y. Lu, Office of Director R24 OD-031467 to Y. Lu and M. Scharl, R2R1 accelerator award from Texas State University to Y. Lu and M. Scharl. RNA-seq data was generated in the Genome Sequencing Facility, which is supported by UT Health San Antonio, NIH-NCI P30 CA054174 (Cancer Center at UT Health San Antonio), NIH-NCI R50 CA265339 and NIH Shared Instrument grant S10OD030311 (S10 grant to NovaSeq 6000 System), CPRIT Core Facility Award (RP220662), and to Z. Lai.

Data Availability Statement

The data that support the findings of this study are available from the corresponding author upon reasonable request.

References

- Abdulsahib, S., W. Boswell, M. Boswell, M. Savage, M. Scharl, and Y. Lu. 2023. "Transcriptional Background Effects on a Tumor Driver Gene in Different Pigment Cell Types of Medaka." *Journal of Experimental Zoology. Part B, Molecular and Developmental Evolution* 342: 252–259. <https://doi.org/10.1002/jez.b.23224>.
- Adam, D., N. Dimitrijevic, and M. Scharl. 1993. "Tumor Suppression in *Xiphophorus* By an Accidentally Acquired Promoter." *Science* 259: 816–819.
- Bateson, W. 1909. "Heredity and Variation in Modern Lights." In *Darwin and Modern Science*, 85–101. Cambridge, UK: Cambridge University Press.
- Coyne, H. A. O. J. 2004. *Speciation*. New York: Sinauer Associates.
- Dobzhansky, T. 1937. *Genetics and the Origin of Species*. New York, NY: Columbia University Press.
- Du, K., Y. Lu, M. Garcia-Olazabal, et al. 2024. "Phylogenomics Analyses of All Species of Swordtails (Genus *Xiphophorus*) Highlights Hybridization Precedes Speciation." *BioRxiv*. <https://doi.org/10.1101/2023.12.30.573732>.
- Gordon, M. 1927. "The Genetics of a Viviparous top-Minnow Platypoecilus; the Inheritance of Two Kinds of Melanophores." *Genetics* 12: 253–283.
- Haiissler, G. 1928. "Über Melanombildungen bei Bastarden von *Xiphophorus helleri* und *Platypoecilus maculatus* var. *Rubra*." *Klinische Wochenschrift* 7, no. 3: 1561–1562. <https://doi.org/10.1093/genetics/12.3.253>.
- He, Y. Y., W. H. Lee, and Y. Zhang. 2004. "Cloning and Purification of Alpha-Neurotoxins From King Cobra (*Ophiophagus hannah*)." *Toxicon* 44: 295–303.

Jumper, J., R. Evans, A. Pritzel, et al. 2021. "Highly Accurate Protein Structure Prediction With AlphaFold." *Nature* 596: 583–589.

Kang, J. H., M. Scharl, R. B. Walter, and A. Meyer. 2013. "Comprehensive Phylogenetic Analysis of All Species of Swordtails and Platies (Pisces: Genus *Xiphophorus*) Uncovers a Hybrid Origin of a Swordtail Fish, *Xiphophorus monticolus*, and Demonstrates That the Sexually Selected Sword Originated in the Ancestral Lineage of the Genus, but Was Lost Again Secondarily." *BMC Evolutionary Biology* 13: 25.

Kazianis, S., H. Gutbrod, R. S. Nairn, et al. 1998. "Localization of a CDKN2 Gene in Linkage Group V of *Xiphophorus* Fishes Defines It as a Candidate for the DIFF Tumor Suppressor." *Genes, Chromosomes & Cancer* 22: 210–220.

Kim, D., G. Pertea, C. Trapnell, H. Pimentel, R. Kelley, and S. L. Salzberg. 2013. "TopHat2: Accurate Alignment of Transcriptomes in the Presence of Insertions, Deletions and Gene Fusions." *Genome Biology* 14: R36.

Kimura, T., Y. Nagao, H. Hashimoto, et al. 2014. "Leucophores Are Similar to Xanthophores in Their Specification and Differentiation Processes in Medaka." *Proceedings of the National Academy of Sciences of the United States of America* 111: 7343–7348.

Koboldt, D. C., K. Chen, T. Wylie, et al. 2009. "VarScan: Variant Detection in Massively Parallel Sequencing of Individual and Pooled Samples." *Bioinformatics* 25: 2283–2285.

Kosswig, C. 1928. "Über Bastarde der Teleostier *Platypoecilus* und *Xiphophorus*." *Zeitschrift für Induktive Abstammungs- und Vererbungslehre* 253: 253.

Kottler, V. A., R. Feron, I. Nanda, et al. 2020. "Independent Origin of XY and ZW Sex Determination Mechanisms in Mosquitofish Sister Species." *Genetics* 214: 193–209.

Langmead, B., and S. L. Salzberg. 2012. "Fast Gapped-Read Alignment With Bowtie 2." *Nature Methods* 9: 357–359.

Li, H. 2011. "A Statistical Framework for SNP Calling, Mutation Discovery, Association Mapping and Population Genetical Parameter Estimation From Sequencing Data." *Bioinformatics* 27: 2987–2993.

Li, H. 2018. "Minimap2: Pairwise Alignment for Nucleotide Sequences." *Bioinformatics* 34: 3094–3100.

Li, H. 2021. "New Strategies to Improve minimap2 Alignment Accuracy." *Bioinformatics* 37: 4572–4574.

Li, H., B. Handsaker, A. Wysoker, et al. 2009. "The Sequence Alignment/Map Format and SAMtools." *Bioinformatics* 25: 2078–2079.

Liao, Y., G. K. Smyth, and W. Shi. 2013. "The Subread Aligner: Fast, Accurate and Scalable Read Mapping by Seed-and-Vote." *Nucleic Acids Research* 41: e108.

Lu, Y., D. Bierbach, J. Ormanns, W. C. Warren, R. B. Walter, and M. Scharl. 2021. "Fixation of Allelic Gene Expression Landscapes and Expression Bias Pattern Shape the Transcriptome of the Clonal Amazon Molly." *Genome Research* 31: 372–379.

Lu, Y., M. Boswell, W. Boswell, et al. 2017. "Molecular Genetic Analysis of the Melanoma Regulatory Locus in *Xiphophorus* Interspecies Hybrids." *Molecular Carcinogenesis* 56: 1935–1944.

Lu, Y., T. J. Olivas, M. Boswell, et al. 2020. "Intra-Strain Genetic Variation of Platyfish (*Xiphophorus maculatus*) Strains Determines Tumorigenic Trajectory." *Frontiers in Genetics* 11: 562594.

Lu, Y., E. Rice, K. du, et al. 2023. "High Resolution Genomes of Multiple *Xiphophorus* Species Provide New Insights Into Microevolution, Hybrid Incompatibility, and Epistasis." *Genome Research* 33: 557–571.

Lu, Y., A. Sandoval, S. Voss, et al. 2020. "Oncogenic Allelic Interaction in *Xiphophorus* Highlights Hybrid Incompatibility." *Proceedings of the National Academy of Sciences of the United States of America* 117: 29786–29794.

- Mack, K. L., and M. W. Nachman. 2017. "Gene Regulation and Speciation." *Trends in Genetics* 33: 68–80.
- Maheshwari, S., and D. A. Barbash. 2011. "The Genetics of Hybrid Incompatibilities." *Annual Review of Genetics* 45: 331–355.
- Meyer, A., J. M. Morrissey, and M. Schartl. 1994. "Recurrent Origin of a Sexually Selected Trait in *Xiphophorus* Fishes Inferred From a Molecular Phylogeny." *Nature* 368: 539–542.
- Monroe, J. D., F. Basheer, and Y. Gibert. 2021. "Xmrks the Spot: Fish Models for Investigating Epidermal Growth Factor Receptor Signaling in Cancer Research." *Cells* 10: 1132.
- Morcinek, J. C., C. Weisser, E. Geissinger, M. Schartl, and C. Wellbrock. 2002. "Activation of STAT5 Triggers Proliferation and Contributes to Anti-Apoptotic Signalling Mediated by the Oncogenic Xmrk Kinase." *Oncogene* 21: 1668–1678.
- Muller, H. 1940. "Bearing of the Drosophila Work on Systematics." In *The New Systematics*, edited by J. Huxley, 185–268. London and New York: Clarendon Press.
- Nairn, R. S., S. Kazianis, B. B. McEntire, L. Della Coletta, R. B. Walter, and D. C. Morizot. 1996. "A CDKN2-Like Polymorphism in *Xiphophorus* LG V Is Associated With UV-B-Induced Melanoma Formation in Platyfish-Swordtail Hybrids." *Proceedings of the National Academy of Sciences of the United States of America* 93: 13042–13047.
- Noor, M. A. 2003. "Evolutionary Biology: Genes to Make New Species." *Nature* 423: 699–700.
- Osipova, E., N. Hecker, and M. Hiller. 2019. "RepeatFiller Newly Identifies Megabases of Aligning Repetitive Sequences and Improves Annotations of Conserved Non-Exonic Elements." *GigaScience* 8: giz132.
- Pennisi, E. 2006. "Evolution. Two Rapidly Evolving Genes Spell Trouble for Hybrids." *Science* 314: 1238–1239.
- Pierce, B., and Z. Weng. 2007. "ZRANK: Reranking Protein Docking Predictions With an Optimized Energy Function." *Proteins* 67: 1078–1086.
- Pierce, B. G., Y. Hourai, and Z. Weng. 2011. "Accelerating Protein Docking in ZDOCK Using an Advanced 3D Convolution Library." *PLoS One* 6: e24657.
- Powell, D. L., M. García-Olazábal, M. Keegan, et al. 2020. "Natural Hybridization Reveals Incompatible Alleles That Cause Melanoma in Swordtail Fish." *Science* 368: 731–736.
- Regneri, J., B. Klotz, B. Wilde, et al. 2019. "Analysis of the Putative Tumor Suppressor Gene *cdkn2ab* in Pigment Cells and Melanoma of *Xiphophorus* and Medaka." *Pigment Cell & Melanoma Research* 32: 248–258.
- Robinson, M. D., D. J. McCarthy, and G. K. Smyth. 2010. "edgeR: A Bioconductor Package for Differential Expression Analysis of Digital Gene Expression Data." *Bioinformatics* 26: 139–140.
- Schartl, M., and Y. Lu. 2024. "Validity of *Xiphophorus* Fish as Models for Human Disease." *Disease Models & Mechanisms* 17: dmm050382.
- Schartl, M., and R. B. Walter. 2016. "*Xiphophorus* and Medaka Cancer Models." *Advances in Experimental Medicine and Biology* 916: 531–552.
- Schartl, M., B. Wilde, J. A. G. C. Laisney, Y. Taniguchi, S. Takeda, and S. Meierjohann. 2010. "A Mutated EGFR Is Sufficient to Induce Malignant Melanoma With Genetic Background-Dependent Histopathologies." *Journal of Investigative Dermatology* 130: 249–258.
- Steinegger, M., and J. Soding. 2017. "MMseqs2 Enables Sensitive Protein Sequence Searching for the Analysis of Massive Data Sets." *Nature Biotechnology* 35: 1026–1028.
- Suarez, H. G., B. E. Langer, P. Ladde, and M. Hiller. 2017. "chain-Cleaner Improves Genome Alignment Specificity and Sensitivity." *Bioinformatics* 33: 1596–1603.
- Sugiyama, A., M. Schartl, and K. Naruse. 2019. "Histopathologic Features of Melanocytic Tumors in *Xiphophorus* Melanoma Receptor Kinase (Xmrk)-transgenic Medaka (*Oryzias latipes*)." *Journal of Toxicologic Pathology* 32: 111–117.
- Tanja, P. K. S., and C. Zerulla. 2021. "The Biology of Polymorphic Melanic Side-Spotting Patterns in Poeciliid Fishes." *Frontiers in Ecology and Evolution* 8: 477.
- Wellbrock, C., P. Fischer, and M. Schartl. 1998. "Receptor Tyrosine Kinase Xmrk Mediates Proliferation in *Xiphophorus* Melanoma Cells." *International Journal of Cancer* 76: 437–442.
- Wellbrock, C., C. Weisser, E. Geissinger, J. Troppmair, and M. Schartl. 2002. "Activation of p59(Fyn) Leads to Melanocyte Dedifferentiation by Influencing MKP-1-Regulated Mitogen-Activated Protein Kinase Signaling." *Journal of Biological Chemistry* 277: 6443–6454.
- Wittbrodt, J., D. Adam, B. Malitschek, et al. 1989. "Novel Putative Receptor Tyrosine Kinase Encoded by the Melanoma-Inducing Tu Locus in *Xiphophorus*." *Nature* 341: 415–421.
- Zheng, W., Z. Li, A. T. Nguyen, C. Li, A. Emelyanov, and Z. Gong. 2014. "Xmrk, Kras and Myc Transgenic Zebrafish Liver Cancer Models Share Molecular Signatures With Subsets of Human Hepatocellular Carcinoma." *PLoS One* 9: e91179.

Supporting Information

Additional supporting information can be found online in the Supporting Information section.